



TECHNICAL ARTICLE

# Effect of Ni/Al Ratio on Solidification Structure and Properties of NiAl-Based Multi-principal Element Alloy

Xicong Ye, Jiaxing Feng, Haofeng Lei, Xin Wu, Dong Fang, Guangwei Zhao, and Bo Li

Submitted: 20 October 2022 / Revised: 24 February 2023 / Accepted: 17 March 2023 / Published online: 17 April 2023

A series of  $(\text{Ni}_x\text{Al})_{65}\text{Cr}_{10}\text{Mo}_5\text{V}_{20}$  ( $x = 0.6, 0.8, 1.0, 1.2, 1.4, 1.6$ ) multi-principal element alloys (MPEAs) (or eutectic high-entropy alloys) were fabricated using a non-self-consumable vacuum melting method, and their solidification microstructures and mechanical properties were examined. As the Ni/Al ratio increases, the microstructure of the alloy changes from hypereutectic (primary BCC + eutectic,  $x = 0.6, 0.8$ ) to eutectic ( $x = 1.0$ ) to hypoeutectic (primary B2 + eutectic,  $x = 1.2, 1.4, 1.6$ ). Within the range of 0.6–1.4, increasing the Ni/Al ratio promotes the production of the B2 phase, and the alloy's fracture strength increases initially and then decreases. The strengthening mechanisms are solid solution strengthening, B2 phase strengthening, and fine-grain strengthening. Among them,  $(\text{Ni}_{1.2}\text{Al})_{65}\text{Cr}_{10}\text{Mo}_5\text{V}_{20}$  exhibits exceptional mechanical properties, with a yield strength of 1600 MPa, a fracture strength of 3106 MPa, a total compression plasticity of 25%, and a hardness of 697 HV. (Ni-1.2, Ni-1.4, and Ni-1.6 show the same mechanical properties within the confidence interval.) Furthermore, the phase prediction criteria for multi-principal element alloys containing Ni and Al were proposed: when  $\Delta H_{\text{mix}} \leq 12.31$  (kJ/mol),  $5.76(\%) \leq \delta_r \leq 7.44(\%)$ , as well as  $0.75 \leq \Omega \leq 1.53$ , the structure of MPEAs is BCC phase + B2 phase.

**Keywords** eutectic high-entropy alloy, mechanical properties, microstructure, multi-principal element alloy, Ni/Al ratio

## 1. Introduction

Multi-principal element alloys (or high-entropy alloys) with multiple main elements and atomic percentages ranging from 5 to 35% have garnered a great deal of attention since their introduction in 2004 (Ref 1, 2). It is well known that single-phased FCC-structured MPEAs have high ductility but low strength (Ref 3–5), whereas BCC-structured MPEAs have low ductility but higher strength. Indeed, a multiphase MPEA (or HEA) with different heat treatments or an appropriate composition design can achieve a combination of strength and plastic toughness (Ref 6–10). Due to the complexity of its composition and the variance in melting point of its components, MPEAs produced by the smelting method often have varying degrees of manufacturing defects and component segregation, stifling MPEAs' industrialization and advancement (Ref 11–13). Lu

(Ref 14) designed  $\text{AlCoCrFeNi}_{2.1}$  MPEA with a composite FCC/B2 structure, which was later defined as EHEA. It has a tensile strength of 1351 MPa and a ductility of 15.4%. This also marks the advent of a revolutionary concept for the design and development of large-scale multi-principal element alloys with high strength and plasticity. Several approaches for designing MEPAs (or EHEAs) have been presented thus far, including mixing enthalpy (Ref 15), simple mixing method (Ref 16), machine learning (Ref 17, 18), phase diagram calculation (CALPHAD) method (Ref 19), and pseudo-binary method (Ref 20).

Due to their low density, high melting point, good thermal conductivity, and great oxidation resistance, NiAl intermetallic compounds have been developed and applied in the field of high-temperature structural materials. However, the brittleness of NiAl-based alloys at room temperature restricts their utilization (Ref 21). Cr, Mo, and V can significantly improve the brittleness of NiAl. For instance, the fracture toughness of NiAl-9Mo (Ref 22, 23), NiAl-32Cr (Ref 24), NiAl-(34-x)Cr-xMo (Ref 25–27), and NiAl-40 V (Ref 28) is higher than that of NiAl intermetallic compounds. In the previous work, research group proposed an infinite solid solution strategy based on the concept of EHEAs (Ref 29). The design idea is that NiAl-34Cr (Ref 30), NiAl-9Mo (Ref 31), and NiAl-39 V (Ref 32) alloys are all eutectic, the microstructures contain the eutectic structure of the NiAl phase and Cr solid solution phase, NiAl phase and Mo solid solution phase, NiAl phase and V solid solution phase, respectively, and V, Cr, and Mo may produce an infinite solid solution with a BCC crystal structure (Ref 33, 34). A series of MEPAs were successfully designed and prepared by incorporating any combination of Cr, Mo, and V into NiAl alloys (Ref 29).

Xicong Ye, Dong Fang, Guangwei Zhao, and Bo Li, Yichang Key Laboratory of Graphite Additive Manufacturing, China Three Gorges University, Yichang 443002, China; and College of Mechanical and Power Engineering, China Three Gorges University, Yichang 443002, China; and Jiaxing Feng, Haofeng Lei, and Xin Wu, College of Mechanical and Power Engineering, China Three Gorges University, Yichang 443002, China. Contact e-mails: yexc@ctgu.edu.cn and hill988@163.com.

Westbrook (Ref 35) and Vedula (Ref 36) found that isometric binary NiAl alloy had substantially lower hardness and strength at room temperature than non-isometric. Qi (Ref 37) compared Ni-30Al-8Mo-2Nb to Ni-40Al-8Mo-2Nb and discovered that the latter had a much better compressive strength given the higher concentration of the NiAl phase. Jin (Ref 38) studied  $\text{CrFeNi}_{3-x}\text{Al}_x$  ( $x = 1, 0.9, 0.8, 0.7, 0.6$ ) MPEAs and discovered that as the Ni/Al ratio increases, the alloy transitions from hypoeutectic to hypereutectic, with enhanced strength and decreased plasticity. As the Ni/Al ratio decreases in  $\text{Al}_x\text{Co}_{15}\text{Cr}_{15}\text{Ni}_{70-x}$  (Ref 38, 39) MPEAs, the alloy shifts from the FCC phase to the BCC + B2 phase as the Ni/Al ratio lowers, and the properties of the alloy alter greatly. Among them,  $\text{Al}_{19.3}\text{Co}_{15}\text{Cr}_{15}\text{Ni}_{50.7}$  had the best overall performance, with a fracture strength of 2850 MPa and a fracture strain of 29%. Changing the Ni/Al ratio to boost performance appears to be a feasible method. In view of the good overall performance of NiAl-10Cr5Mo20V (Ref 29) in the previous work, this work explored optimizing the alloy by adjusting the Ni/Al ratio and studying the solidification microstructure and alloy properties.

## 2. Experimental

The multi-principal element alloys  $(\text{Ni}_x\text{Al})_{65}\text{Cr}_{10}\text{Mo}_5\text{V}_{20}$  ( $x = 0.6, 0.8, 1.0, 1.2, 1.4$  and  $1.6$ ) (referred to as Ni-0.6, Ni-0.8, Ni-1.0, Ni-1.2, Ni-1.4 and Ni-1.6) were produced using raw materials with  $\geq 99.5\%$  purity level in a high-purity argon environment. To ensure consistency, each sample underwent at least six separate melting. The samples were cleaned with sandpaper to eliminate surface oxides before detecting crystal structures with XRD utilizing  $\text{CuK}\alpha$  radiation at 40 kV/40 mA and a scanning rate of  $4^\circ/\text{min}$  from  $20$  to  $100^\circ$ . After polishing, the samples were etched with aqua regia (nitric acid/hydrochloric acid = 1:3 V%), and the microstructure and elemental distribution of the alloys were determined using SEM-EDS. At room temperature, a WDW-100E universal testing machine was used to compress a  $\text{Ø}3*6$  (mm) cylinder at a strain rate of  $5 \times 10^{-4} \text{ s}^{-1}$ . In order to eliminate measurement error, each sample was tested six times in ten seconds using a Vickers hardness tester (MH-6L) with a force of 100N.

## 3. Results and Discussion

### 3.1 Crystal Structure

Figure 1 depicts the XRD patterns of the as-cast  $(\text{Ni}_x\text{Al})_{65}\text{Cr}_{10}\text{Mo}_5\text{V}_{20}$  ( $x = 0.6, 0.8, 1.0, 1.2, 1.4, 1.6$ ) MPEAs, indicating that all of the alloys are B2 + BCC phase. Table 1 shows the binary mixing enthalpy of each element. As Ni and Al have the largest negative binary mixing enthalpy, they tend to form the NiAl intermetallic complex B2; V, Cr, and Mo have practically zero mixing enthalpy and can form an infinite solid solution BCC phase. It is hypothesized that the volume fraction of the B2 phase varies with the Ni/Al ratio based on the intensity relationship of the distinctive peaks corresponding to the B2 phase and the BCC phase exhibited in Fig. 1(a) from  $40$  to  $50^\circ$ . The B2 phase grows with a Ni/Al ratio between  $0.6$  and  $1.4$ . When compared to the alloy structure with Ni-1.4, the B2 phase decreases slightly when the Ni-1.6; Fig. 1(b) is a partially

enlarged plot of Fig. 1(a) from  $75$  to  $85^\circ$ . Table 2 displays the computed lattice constants using the Bragg equation for the BCC(211) and B2(211) phases. The characteristic peaks of the BCC phase shift to a high angle as the Ni/Al ratio grows, and the lattice constant decreases; the Ni/Al ratio has little influence on the characteristic peaks of the B2 phase.

### 3.2 Microscopic Characteristics

Figure 2 displays the SEM picture of  $(\text{Ni}_x\text{Al})_{65}\text{Cr}_{10}\text{Mo}_5\text{V}_{20}$  MPEAs, and Table 3 summarizes the findings of the SEM-EDS study data. Figure 2(a) and (b) presents a white-gray alternating layered lamellar structure in a Ni-0.6 hypereutectic multi-principal element alloy. When combined with the data in Table 3, the gray phase is identified as the Ni- and Al-rich B2 phase, whereas the white phase is identified as the V-, Cr-, and Mo-rich BCC phase. During the solidification of the Ni-0.6 alloy, the BCC phase precipitates as a primary crystal with a volume fraction of approximately 26.5% and dendritic characteristics. The remaining liquid phase changes into a layered eutectic tissue consisting of white and gray phases. Figure 2(c), (d), (e), and (f) exhibits SEM images of Ni-0.8 and Ni-1.0. In Ni-0.8, the volume fraction of the primary BCC phase is reduced by up to 11.8%, and the eutectic layer is refined, indicating that this proportion is close to the eutectic point. In Ni-1.0 alloys, the typical eutectic organization is observed, with eutectic dendrites consisting of alternating NiAl and VCrMo lamellae, that is, alternating B2 and BCC phases. In a radial pattern extending outward from the interior to the cell or dendrite boundary, the lamellae at the grain boundaries ( $\sim 640$  nm) are coarser than those in the interior ( $\sim 430$  nm). This is due to the heat emitted by the solidification of the pro-eutectic clot affecting the eutectic tissue at the grain boundaries. Figure 2(g) and (h) shows an as-cast SEM image of the Ni-1.2 alloy. The gray dendrites in the image represent the primary B2 phase, which is relatively coarse due to direct crystallization from the liquid phase, and the gray-white interphase tissue distributed in the dendritic interstices is the BCC + B2 eutectic. Figure 2(i), (j), (k), and (l) shows SEM images of Ni-1.4 and Ni-1.6, which are also hypoeutectic alloys and have the same structure as Ni-1.2. As the Ni/Al ratio increases, the gray dendrites get coarser and the volume fraction of eutectic tissue decreases.

Figure 2 demonstrates that when the Ni/Al ratio increases, the eutectic organization transitions from irregular to regular back to irregular, and the  $(\text{Ni}_x\text{Al})_{65}\text{Cr}_{10}\text{Mo}_5\text{V}_{20}$  alloy system also changes from hypereutectic ( $x = 0.6, 0.8$ ) to eutectic ( $x = 1.0$ ) and then finally to hypoeutectic ( $x = 1.2, 1.4, 1.6$ ). The B2 phase volume fraction increases with the Ni/Al ratio, peaking at 67.5% in Ni-1.4 and decreasing to 61.3% in Ni-1.6, a trend that is consistent with the XRD results. This is because as the Ni/Al ratio increases, the amount of Ni increases while the amount of Al decreases. The B2 phase content reaches its maximum at 1.4, not at 1.0, due to the fact that Ni and Al have differing solid solubility in the BCC phase, and when Ni increases again, the decrease of Al causes the B2 phase content of Ni-1.6 to fall. Since the atomic radius of Al is substantially larger than that of V, Cr, and Mo, the magnitude of the lattice constant of BCC phase is proportional to the solid solution Al content in BCC phase. As the Ni/Al ratio rises, the BCC phase contains less Al and the lattice constant increases. According to the Bragg equation, the lattice constant decreases and the angle increases, this can explain the shift of the BCC phase peak

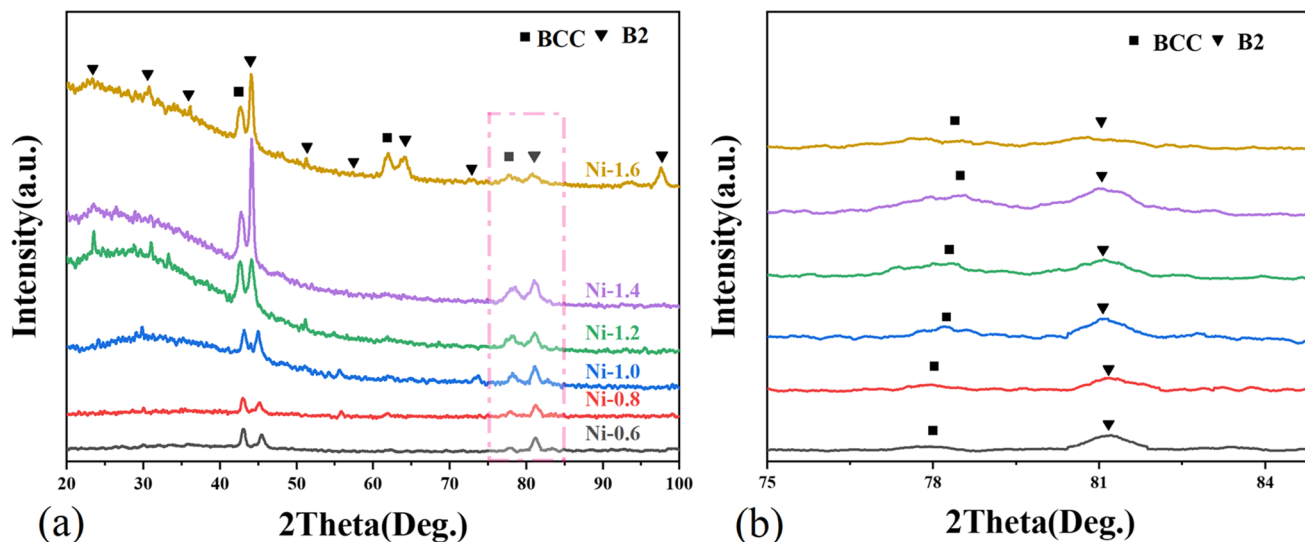


Fig. 1 XRD diagram of the  $(\text{Ni}_x\text{Al})_{65}\text{Cr}_{10}\text{Mo}_5\text{V}_{20}$  ( $x = 0.6, 0.8, 1.0, 1.2, 1.4, 1.6$ ) MPEAs. (a) as-cast; (b) enlarged from 75 to 85°

**Table 1 Binary enthalpy of mixing of elements in alloys (KJ/mol)**

Mixing enthalpy	Ni	Al	V	Cr	Mo
Ni	...	- 22	- 18	12	- 7
Al		...	- 16	- 10	- 5
V			...	- 2	0
Cr				...	0
Mo					...

**Table 2 The BCC and B2 phase lattice constants in  $(\text{Ni}_x\text{Al})_{65}\text{Cr}_{10}\text{Mo}_5\text{V}_{20}$  ( $x = 0.6, 0.8, 1.0, 1.2, 1.4, 1.6$ ) MPEAs**

Alloys	Lattice parameters, Å	
	BCC	B2
Ni-0.6	2.9699	2.8788
Ni-0.8	2.9689	2.8786
Ni-1.0	2.9675	2.8785
Ni-1.2	2.9677	2.8784
Ni-1.4	2.9664	2.8784
Ni-1.6	2.9668	2.8784

toward higher angles and the drop in lattice constant in XRD. Meanwhile, gray precipitate was observed in the BCC phase and white precipitate was observed in the B2 phase, which was caused by the hysteretic diffusion effect, and the quick cooling mode of the water-cooled copper crucible would aggravate the hysteresis diffusion, as Wang et al. (Ref 40-42) anticipated. The alloy's eutectic point is  $x = 1.0$ , which is consistent with previous experimental results (Ref 29). Figure 3 illustrates the elemental distribution of  $(\text{Ni}_x\text{Al})_{65}\text{Cr}_{10}\text{Mo}_5\text{V}_{20}$  MPEAs, with V, Cr, and Mo more concentrated in the primary BCC phase in the hypereutectic organization (a) and (b), and Ni and Al more concentrated in the primary B2 phase in hypoeutectic organization (d), (e), and (f).

### 3.3 Mechanical Properties

Figure 4 depicts the compressive stress-strain curve for the  $(\text{Ni}_x\text{Al})_{65}\text{Cr}_{10}\text{Mo}_5\text{V}_{20}$  ( $x = 0.6, 0.8, 1.0, 1.2, 1.4, 1.6$ ) MPEAs. Table 4 shows the alloy's room-temperature compression properties and microhardness. Ni-0.6 exhibited high brittleness with a fracture strength and fracture strain of 1519 MPa and 7%, respectively. The alloy's yield strength and fracture strength tend to rise when the Ni/Al ratio changes, although Ni-1.2 had the highest fracture strength while Ni-1.4 and Ni-1.6 decreased, with fracture strengths of 3093 and 3058 MPa, respectively. All of the alloys in the system had a strain at break of more than 22%, except for Ni-0.6, which was extremely brittle. The alloy system's high compressive strength can be explained as follows: As the Ni/Al ratio increases, the eutectic lamellae spacing or primary crystals become finer and eventually coarser, with lower eutectic lamellae spacing in the Ni/Al ratio range of 0.8 to 1.2. With the increase of B2 phase, the B2 phase is an intermetallic compound with a greater strength than the BCC phase. The alloys with BCC/B2 coherent structure that have a matrix that is B2 phase have higher strength in general (Ref 43). The hardness of the primary B2 phase in Fig. 5(a) is greater than that of the primary BCC phase, and when combined with Fig. 5(b) and the change in alloy fracture strength, it may be assumed that the B2 phase is the alloy system's strengthening phase.  $(\text{Ni}_x\text{Al})_{65}\text{Cr}_{10}\text{Mo}_5\text{V}_{20}$  has more B2 phase when the Ni/Al ratio is between 1.2 and 1.6 and has the most B2 phase at Ni-1.4. Precipitation strengthening: the nano-sized BCC phase precipitated within the B2 phase, and the nano-sized B2 phase precipitated within the BCC phase might enhance the material's strength, but the mechanism of the actions requires additional research and discussion. The effect of solid solution strengthening is gradually weakened as the Ni/Al ratio increases, as seen by a drop in Al content in the BCC phase and the decrease in the lattice constant of the BCC phase, implying that the B2 phase is getting larger.

When the Ni/Al ratio was increased from 0.6 to 0.8, the fracture strength and fracture strain of the Ni-0.8 alloy increased substantially. It could be due to the expansion of the B2 phase and the refinement of the eutectic structure. When the Ni/Al ratio is 1.0, the eutectic layer continues to refine,

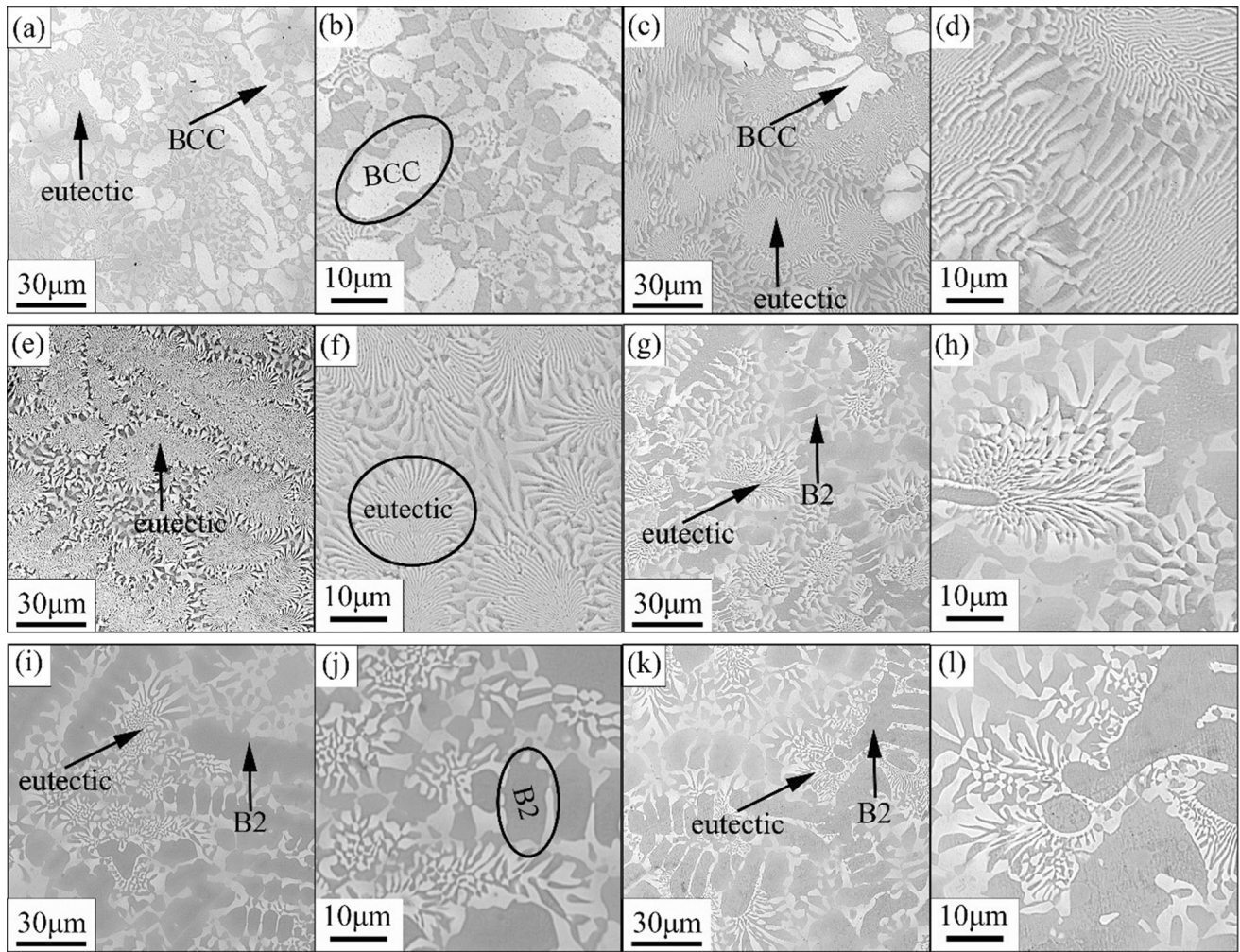


**Fig. 2**  $(\text{Ni}_x\text{Al})_{65}\text{Cr}_{10}\text{Mo}_5\text{V}_{20}$  MPEAs SEM images: (a-b) Ni-0.6; (c-d) Ni-0.8; (e-f) Ni-1.0; (g-h) Ni-1.2; (i-j) Ni-1.4; (k-l) Ni-1.6

**Table 3** Distribution of different phases of elements in  $(\text{Ni}_x\text{Al})_{65}\text{Cr}_{10}\text{Mo}_5\text{V}_{20}$  MPEAs

Alloys	Phase	Al, at.%	Ni, at.%	V, at.%	Cr, at.%	Mo, at.%
Ni-0.6	Eutectic	40.56	31.60	15.51	8.13	4.20
	BCC	29.24	7.45	34.65	17.04	11.61
	B2	48.19	47.71	2.04	1.65	0.41
Ni-0.8	Eutectic	33.43	30.17	20.14	10.43	5.82
	BCC	26.78	16.28	35.31	16.67	4.96
	B2	43.78	44.54	7.27	3.61	0.80
Ni-1.0	Eutectic	34.64	32.74	17.42	9.27	5.93
	BCC	17.67	14.44	35.27	18.10	8.53
	B2	39.76	41.31	14.10	5.21	0.63
Ni-1.2	Eutectic	25.77	27.58	21.34	14.80	10.52
	BCC	13.82	19.39	36.75	20.76	10.28
	B2	36.99	50.80	8.06	3.48	0.67
Ni-1.4	Eutectic	18.05	30.06	25.41	14.85	11.64
	BCC	11.69	20.68	36.46	19.45	11.71
	B2	36.42	48.98	8.91	4.35	1.34
Ni-1.6	Eutectic	20.20	22.60	26.93	16.04	14.23
	BCC	9.96	17.80	37.92	20.83	13.48
	B2	36.10	48.94	8.47	4.69	1.81

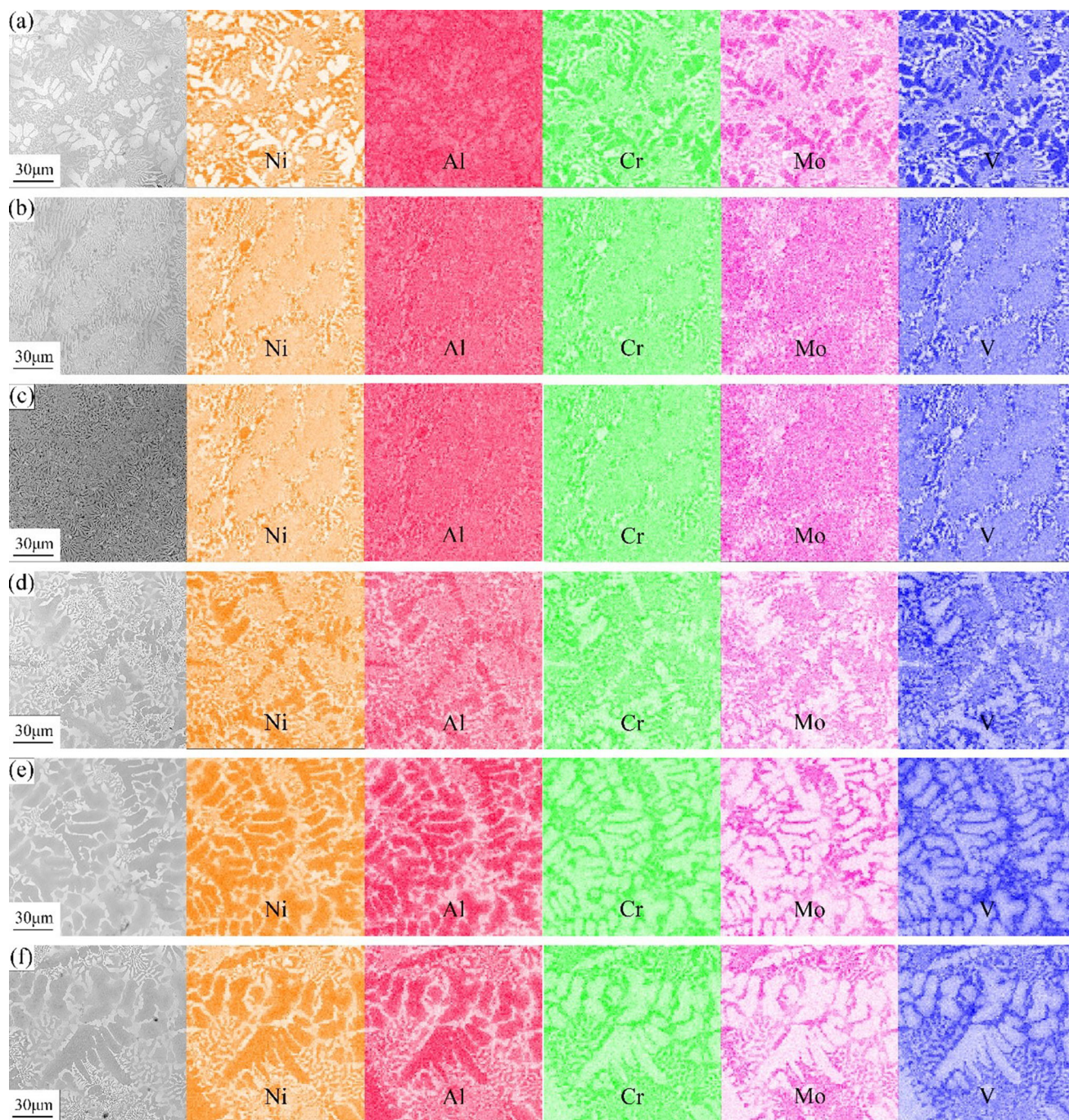


**Fig. 3** EDS analysis findings for  $(\text{Ni}_x\text{Al})_{65}\text{Cr}_{10}\text{Mo}_5\text{V}_{20}$  MPEAs: (a) Ni-0.6; (b) Ni-0.8; (c) Ni-1.0; (d) Ni-1.2; (e) Ni-1.4; (f) Ni-1.6

especially the irregular layer spacing at the grain boundary, which changes from about 520 nm for Ni/Al of 0.8 to about 430 nm for Ni/Al of 1.0. As a result, the fine-grain strengthening and the increase in the B2 phase result in higher fracture strength and compression. The Ni-1.2 alloy is transformed from eutectic to hypoeutectic with a primary B2 phase volume fraction of about 23.1% and a coarsened lamellae organization with a spacing of about 630 nm. Therefore, the strengthening mechanism of Ni-1.2 alloy is mainly B2 phase strengthening compared to Ni-1.0 alloy, but the coarsened lamellae spacing results in a slight decrease in compressibility. The fracture strength and hardness of Ni-1.4 decrease, which may be due to

the coarsening of eutectic lamellar ( $\sim 740$  nm) and irregularity, and the negative impacts of BCC phase lattice constant drop outweigh the strengthening effect of B2 phase increase. In Ni-1.6, the B2 phase is reduced and the eutectic lamellar does not change much ( $\sim 720$  nm), which lowers the alloy's fracture strength. Simultaneously, we find that precipitation strengthening is prevalent throughout the alloy system, as can be demonstrated in Fig. 3. In summary, the strengthening and toughening mechanism of the alloy is a competing process of fine-grain strengthening, precipitation strengthening, B2 phase strengthening, and solid solution strengthening, with Ni-1.2 having the best overall mechanical properties.

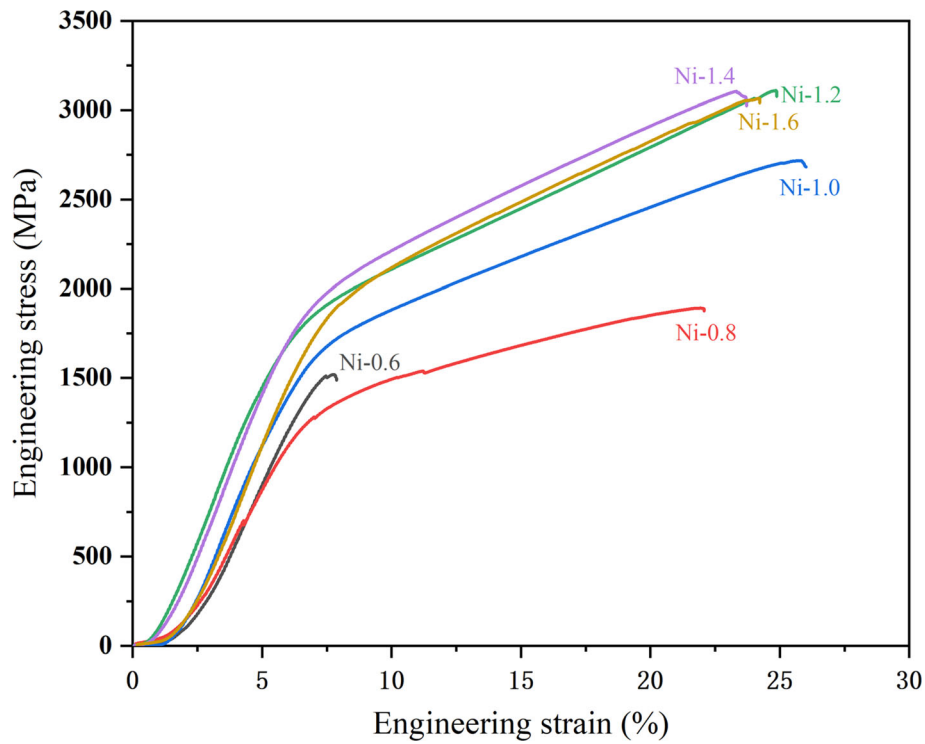


**Fig. 4** Room-temperature  $(\text{Ni}_x\text{Al})_{65}\text{Cr}_{10}\text{Mo}_5\text{V}_{20}$  MPEAs compressive strength group

**Table 4** Room-temperature compression of  $(\text{Ni}_x\text{Al})_{65}\text{Cr}_{10}\text{Mo}_5\text{V}_{20}$  MPEAs

MPEAs	$\sigma_{0.2}$ , MPa	$\sigma_p$ , MPa	$\epsilon_p$ , %	HV
Ni-0.6	1394 ± 47	1519 ± 44	7 ± 2	575 ± 15
Ni-0.8	1381 ± 44	1893 ± 64	22 ± 1	587 ± 9
Ni-1.0	1474 ± 20	2718 ± 37	26 ± 1	666 ± 5
Ni-1.2	1600 ± 54	3106 ± 45	25 ± 1	697 ± 22
Ni-1.4	1648 ± 31	3093 ± 86	23 ± 1	684 ± 29
Ni-1.6	1611 ± 24	3058 ± 114	24 ± 1	677 ± 28

### 3.4 Relationship Between Microstructure and Mechanical Properties

The mechanical traits of  $(\text{Ni}_x\text{Al})_{65}\text{Cr}_{10}\text{Mo}_5\text{V}_{20}$  MPEAs are significantly affected by changes in the Ni/Al ratio. Figure 6 demonstrates the outcome of the B2 phase volume fraction change on the yield strength of  $(\text{Ni}_x\text{Al})_{65}\text{Cr}_{10}\text{Mo}_5\text{V}_{20}$  MPEAs, signifying that the B2 phase could yield a good strengthening action. The strength of the multi-principal element alloy can be roughly expressed using the prediction law of mixtures (Ref 44) in the eutectic structure formed by the hard B2 phase and the BCC solid solution with good toughness:

$$\begin{aligned} \sigma_{0.2} &= \sigma_{B2}V_{B2} + \sigma_{BCC}(1 - V_{B2}) \\ &= \sigma_{BCC} + (\sigma_{B2} - \sigma_{BCC})V_{B2} \end{aligned} \quad (\text{Eq 1})$$

Corresponding strain assumptions are devised in this work, where  $V_{B2}$  refers to the volume fraction of the B2 phase, while  $\sigma_{0.2}$ ,  $\sigma_{B2}$ , and  $\sigma_{BCC}$  represent the stresses of alloy respectively.  $\sigma_{BCC}$  and  $\sigma_{B2}$  are constant values. The fitting curve of the alloy shows a good linear relationship with the yield strength, and the

increase of B2 phase has a positive contribution to the yield strength.

To accurately assess the contribution of the strengthening mechanism to the overall performance, it is essential to calculate the solid solution strengthening of the  $(\text{Ni}_x\text{Al})_{65}\text{Cr}_{10}\text{Mo}_5\text{V}_{20}$  alloy. This alloy can be considered a VCrMo solvent with Ni and Al acting as solutes that are partially soluble in VCrMo. As a result, the solution strengthening can be expressed using a displacement solution strengthening model that is based on dislocation-solute interactions (Ref 45, 46):

$$\Delta\delta_s = M \cdot \frac{G \cdot \epsilon_s^{3/2} \cdot c^{1/2}}{700} \quad (\text{Eq 2})$$

The shear modulus ( $G$ ) of the NiAl system can be calculated for the  $(\text{Ni}_x\text{Al})_{65}\text{Cr}_{10}\text{Mo}_5\text{V}_{20}$  alloy using a simple mixing rule (Ref 47), assuming that the alloy is an isotropic solid. Here,  $c$  represents the total molar percentage of Ni and Al in the BCC matrix. The mean orientation factor for the polycrystalline matrix in the BCC phase is  $M = 2.9$  (Ref 47), and the interaction parameter ( $\epsilon_s$ ) can be expressed as:

$$\epsilon_s = \left| \frac{\epsilon_G}{1 + 0.5\epsilon_G} - 3 \cdot \epsilon_a \right| \quad (\text{Eq 3})$$

This equation combines the effects of elastic and atomic size mismatch, represented by  $\epsilon_G$  and  $\epsilon_a$ , respectively. Specifically,  $\epsilon_G$  and  $\epsilon_a$  are defined as:

$$\epsilon_G = \frac{1}{G} \frac{\partial G}{\partial c} \quad (\text{Eq 4})$$

$$\epsilon_a = \frac{1}{a} \frac{\partial a}{\partial c} \quad (\text{Eq 5})$$

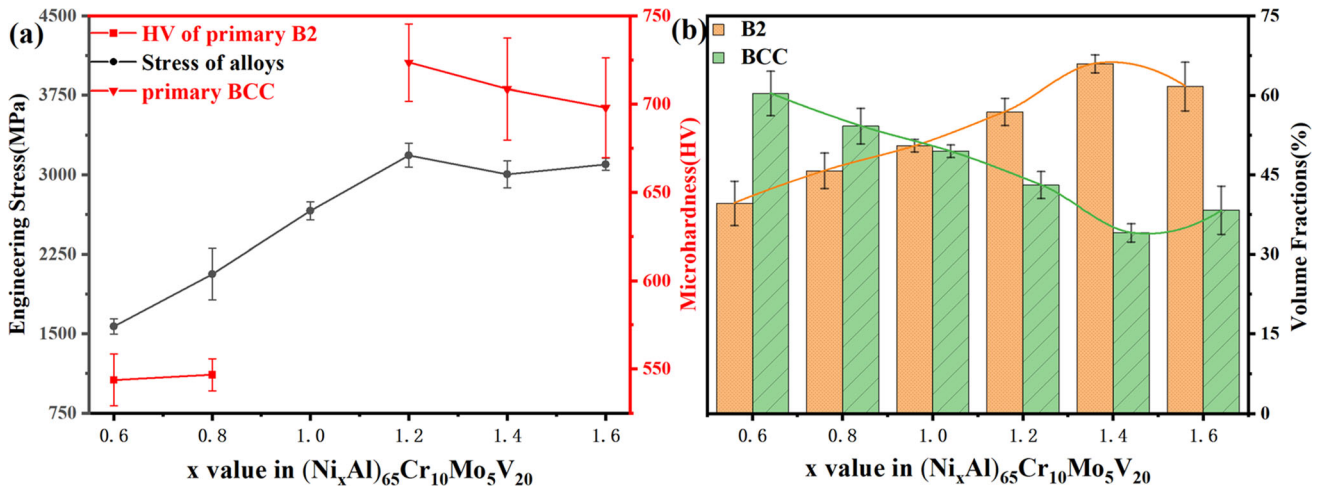


**Fig. 5** (a) The hardness of primary phase and stress of  $(\text{Ni}_x\text{Al})_{65}\text{Cr}_{10}\text{Mo}_5\text{V}_{20}$  MPEAs; (b) Volume fraction of primary phase in  $(\text{Ni}_x\text{Al})_{65}\text{Cr}_{10}\text{Mo}_5\text{V}_{20}$  MPEAs

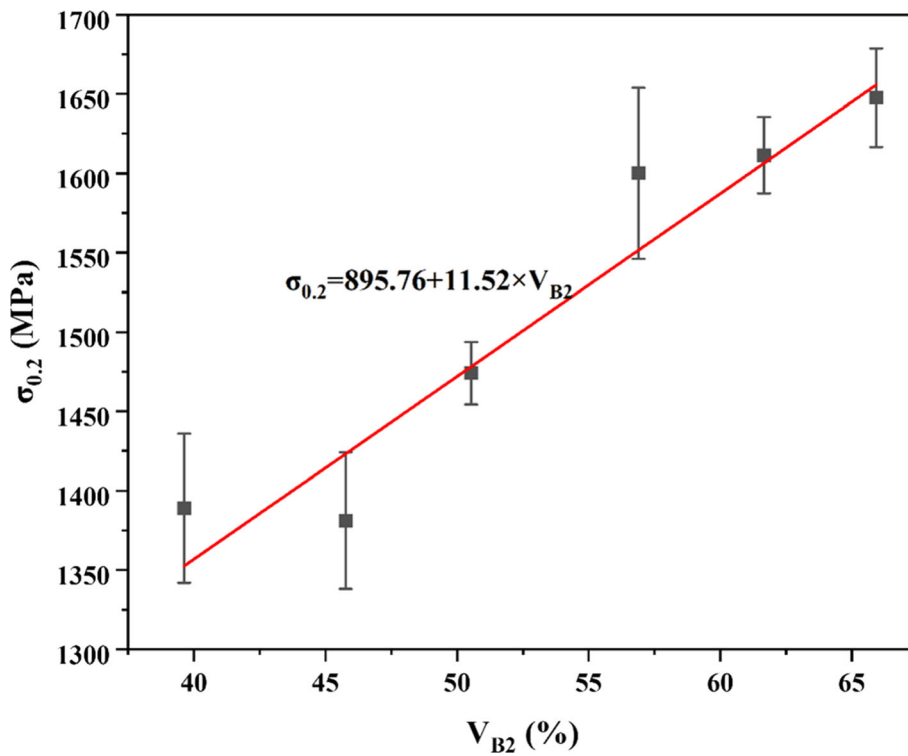


**Fig. 6** Relationship between volume fraction of B2 phase and yield strength in  $(\text{Ni}_x\text{Al})_{65}\text{Cr}_{10}\text{Mo}_5\text{V}_{20}$  MPEAs

The parameter  $\varepsilon_G$  can be neglected in comparison with  $\varepsilon_a$ , while the parameter  $a$  can be determined from the lattice constants provided in Table 2 for the BCC phase. The contribution values for solid solution strengthening from Ni-0.6 to Ni-1.6 are as follows, in order: 58.6, 59.1, 55.3, 56.4, 55.8, and 51.9 MPa. These results indicate that the impact of solid solution strengthening on the strength of the alloy is relatively small.

When the grain size is smaller, the grain boundary area will be larger, and the slip resistance of the dislocation near the grain boundary becomes greater; thus, it can be concluded that finer grain size enhances strength. Literature has reported that the correlation between the yield strength and grain size of

polycrystalline materials can be expressed with the following classical Hall–Petch equation (Ref 48, 49):

$$\Delta\delta_y = k/\lambda^{1/2} \quad (\text{Eq 6})$$

where  $\Delta\delta_y$  is expressed as yield stress,  $k$  is the constant. In the case of  $(\text{Ni}_x\text{Al})_{65}\text{Cr}_{10}\text{Mo}_5\text{V}_{20}$  MPEAs, the secondary dendrite spacing and grain size would reduce following the introduction of B2. In this study, the parameter  $k = 628 \text{ MPa}\cdot\mu\text{m}^{1/2}$  was employed to assess the contribution of fine crystal strengthening (Ref 50). The calculated increase in yield strength was 957 MPa and 730 MPa for Ni-1.0 with the smallest grain size (eutectic structure) and Ni-1.4 with the largest grain size,

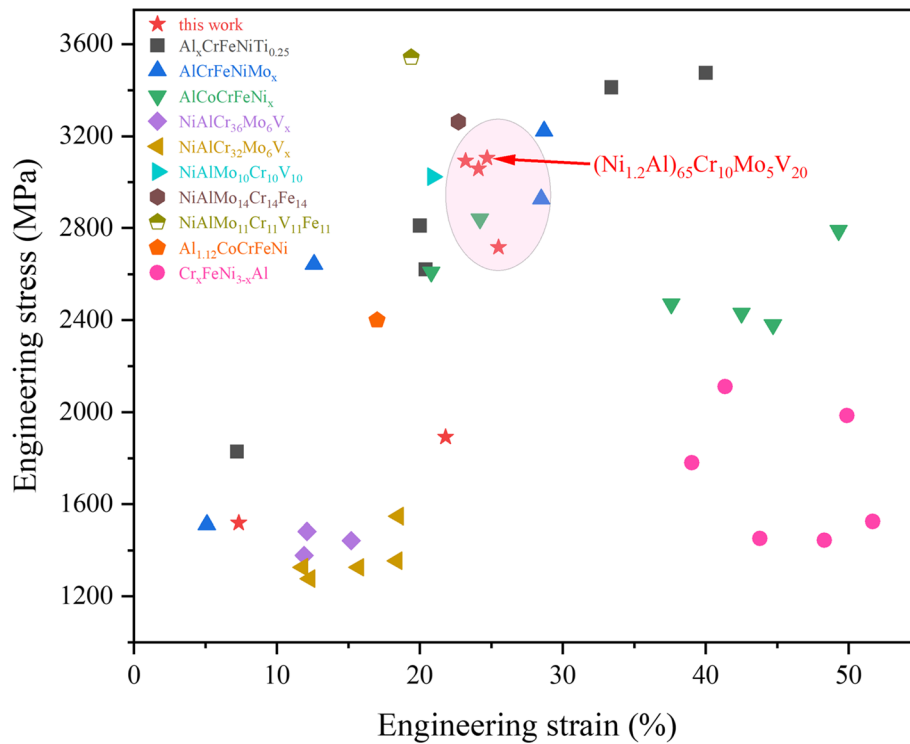


**Fig. 7**  $(\text{Ni}_x\text{Al})_{65}\text{Cr}_{10}\text{Mo}_5\text{V}_{20}$  MPEAs and HEAs with similar structure compression strength comparison graph

respectively, hinting that fine-grain strengthening plays a significant part in the alloy system. To conclude, the main factors contributing to the strengthening of the alloy system include the addition of the B2 phase as well as fine-grain strengthening.

Ni-1.2, Ni-1.4, and Ni-1.6 all possess high strength, with Ni-1.2 exhibiting relatively better plasticity. The increase in strength is mostly attributable to a rise in the B2 phase and fine-grain strengthening of the eutectic group. The increment of the hard B2 phase can limit dislocation and interface migration effectively. At the same time, the precipitate produced during solidification promotes the nucleation of eutectic masses while inhibiting grain development. The refined eutectic lamellae is made up of more interfaces, contributing to the inhibition of dislocation motion and promotes strength improvement. There are two plausible contributors for the increase in plasticity. The fundamental explanation is the fine-tuning of the eutectic lamellae when there is an increment in the Ni/Al ratio (as shown in Fig. 2). The eutectic structure's grain refinement disperses plastic deformation across more grains, thus decreasing stress concentration and improving plasticity. The main reason for the relatively better plasticity of Ni-1.2 is the refinement of the eutectic lamellar structure due to the increase in the Ni/Al ratio, as shown in Fig. 2. With the grain refinement of the eutectic microstructure, plastic deformation is dispersed over more grains, resulting in less stress concentration and higher ductility.

In conjunction with numerous published research, this study collated the mechanical properties of several MPEAs (or HEAs) with comparable structures, as shown in Fig. 7. AlCoCrFeNi with the same BCC + B2 structure as the alloys studied in this work has a strength and plasticity close to Ni-1.0, but lower than Ni-1.2, Ni-1.4, and Ni-1.6. It is worth noting that AlCoCrFeNiMo<sub>0.2</sub> (Ref 51) has a BCC + B2 structure with

slightly lower plasticity and strength than Ni-1.2, both with excellent all-round properties, but its yield strength and hardness are nearly 11% lower than Ni-1.2. NiAlMo<sub>10</sub>Cr<sub>10</sub>V<sub>10</sub>, NiAlMo<sub>14</sub>Cr<sub>14</sub>Fe<sub>14</sub>, and NiAlMo<sub>11</sub>Cr<sub>11</sub>V<sub>11</sub>Fe<sub>11</sub> (Ref 52) are also made up of BCC + B2, which have high strength but only around 20% plasticity. The yield strength of NiAl-Cr(Mo)-0.5Hf alloy is only 1380 MPa, which is substantially lower than the 1600 MPa of Ni-1.2 (Ref 53); it is regarded as a conventional high-strength alloy. The mechanical properties of Ni-1.2 alloy are not inferior to those of multi-principal element alloys of the same type, making it a promising new structural material.

### 3.5 Phase Prediction

Table 5 calculates the relevant thermodynamic parameters of  $(\text{Ni}_x\text{Al})_{65}\text{Cr}_{10}\text{Mo}_5\text{V}_{20}$  and some typical cast eutectic high-entropy alloys, as follows:

$$\delta = \sqrt{\sum_{i=1}^n c_i(1 - r_i/\bar{r})^2}, \bar{r} = \sum_{i=1}^n c_i r_i \quad (\text{Eq 7})$$

$$\Delta H_{\text{mix}} = \sum_{i=1, i \neq j}^n 4\Delta H_{ij}^{\text{mix}} c_i c_j \quad (\text{Eq 8})$$

$$\Omega = T_m \Delta S_{\text{mix}} / |\Delta H_{\text{mix}}|, T_m = \sum_{i=1}^n c_i (T_m)_i \quad (\text{Eq 9})$$

where n represents the total number of atoms, r represents the mean atomic radius,  $c_i$  represents the fraction of atoms belonging to element  $i$ ,  $r_i$  represents its radius,  $\Delta H_{ij}$  represents the enthalpy of mixing between elements  $i$  and  $j$ , and  $(T_m)_i$  represents its melting point.



**Table 5** Calculation results of physical parameters of Ni, Al containing MPEAs

MPEAs	$\delta_r$ , %	VEC	$\Delta H$ , kJ/mol	$\Delta S$ , J/k mol	$\Omega$	Phase	References
(Ni <sub>0.6</sub> Al) <sub>65</sub> Cr <sub>10</sub> Mo <sub>5</sub> V <sub>20</sub>	6.79	5.56	- 20.64	11.74	0.75	BCC + B2	This work
(Ni <sub>0.8</sub> Al) <sub>65</sub> Cr <sub>10</sub> Mo <sub>5</sub> V <sub>20</sub>	6.87	5.87	- 21.14	11.87	0.76	BCC + B2	
(Ni <sub>1.0</sub> Al) <sub>65</sub> Cr <sub>10</sub> Mo <sub>5</sub> V <sub>20</sub>	6.88	6.13	- 21.28	11.91	0.77	BCC + B2	
(Ni <sub>1.2</sub> Al) <sub>65</sub> Cr <sub>10</sub> Mo <sub>5</sub> V <sub>20</sub>	6.85	6.33	- 21.23	11.89	0.79	BCC + B2	
(Ni <sub>1.4</sub> Al) <sub>65</sub> Cr <sub>10</sub> Mo <sub>5</sub> V <sub>20</sub>	6.80	6.55	- 21.07	11.83	0.80	BCC + B2	
(Ni <sub>1.6</sub> Al) <sub>65</sub> Cr <sub>10</sub> Mo <sub>5</sub> V <sub>20</sub>	6.74	6.65	- 20.85	11.76	0.81	BCC + B2	
AlCoCrFeNi	5.78	7.20	- 12.32	13.38	1.53	BCC + B2	(Ref 39)
AlCoCrFeNi <sub>1.5</sub>	5.59	7.45	- 12.23	13.25	1.53	BCC + FCC + B2	
AlCoCrFeNi <sub>1.8</sub>	5.48	7.58	- 12.10	13.09	1.53	FCC + B2	
AlCoCrFeNi <sub>2.1</sub>	5.38	7.70	- 11.94	12.91	1.53	FCC + B2	
AlCoCrFeNi <sub>2.4</sub>	5.19	7.81	- 11.76	12.70	1.53	FCC + B2	
AlCoCrFeNi <sub>3.0</sub>	5.10	8.00	- 11.35	12.26	1.53	FCC + B2	
Al <sub>0.25</sub> CrFeNiTi <sub>0.25</sub>	5.51	7.36	- 12.21	12.06	1.54	BCC + FCC + B2	(Ref 54)
Al <sub>0.5</sub> CrFeNiTi <sub>0.25</sub>	6.27	7.08	- 14.25	12.53	1.32	BCC + B2	
Al <sub>0.75</sub> CrFeNiTi <sub>0.25</sub>	6.75	6.81	- 15.65	12.69	1.17	BCC + B2	
AlCrFeNiTi <sub>0.25</sub>	7.07	6.58	- 16.63	12.70	1.07	BCC + B2	
Al <sub>1.12</sub> CoCrFeNi	6.51	7.09	- 12.86	13.36	1.44	BCC + B2	
NiAlCr <sub>32</sub> Mo <sub>6</sub>	7.44	6.31	- 16.09	10.47	0.92	BCC + B2	(Ref 42)
NiAlCr <sub>32</sub> Mo <sub>6</sub> V <sub>0.5</sub>	7.41	6.30	- 16.12	10.68	0.94	BCC + B2	
NiAlCr <sub>32</sub> Mo <sub>6</sub> V <sub>1</sub>	7.39	6.29	- 16.14	10.84	0.96	BCC + B2	
NiAlCr <sub>32</sub> Mo <sub>6</sub> V <sub>2</sub>	7.35	6.28	- 16.18	11.09	0.98	BCC + B2	
NiAlCr <sub>32</sub> Mo <sub>6</sub> V <sub>3</sub>	7.31	6.30	- 16.21	11.30	1.01	BCC + B2	
NiAlCr <sub>36</sub> Mo <sub>6</sub>	7.34	6.29	- 15.33	10.47	0.99	BCC + B2	
NiAlCr <sub>36</sub> Mo <sub>6</sub> V <sub>0.5</sub>	7.32	6.28	- 15.35	10.64	1.01	BCC + B2	
NiAlCr <sub>36</sub> Mo <sub>6</sub> V <sub>1</sub>	7.30	6.27	- 15.36	10.79	1.02	BCC + B2	
AlCrFeNi	5.76	6.75	- 13.25	11.53	1.20	BCC + B2	(Ref 43)
AlCrFeNiMo <sub>0.2</sub>	5.78	6.71	- 12.65	12.57	1.43	BCC + B2	
AlCrFeNiMo <sub>0.5</sub>	5.79	6.67	- 11.85	13.15	1.69	BCC + B2 + $\sigma$	
AlCrFeNiMo <sub>0.8</sub>	5.76	6.63	- 11.15	13.35	1.90	BCC + $\sigma$	
AlCrFeNiMo	5.73	6.60	- 10.72	13.38	2.04	BCC + $\sigma$	
Fe <sub>20</sub> Co <sub>20</sub> Ni <sub>41</sub> Al <sub>19</sub>	5.96	8.07	- 12.23	11.01	1.08	L12 + B2	(Ref 55)
NiAlMo <sub>10</sub> Cr <sub>10</sub> V <sub>10</sub>	7.42	6.25	- 19.68	11.85	1.44	BCC + B2	(Ref 52)
NiAlMo <sub>14</sub> Cr <sub>14</sub> Fe <sub>14</sub>	7.08	6.15	- 14.45	12.83	1.14	BCC + B2	
NiAlMo <sub>11</sub> Cr <sub>11</sub> V <sub>11</sub> Fe <sub>11</sub>	6.81	6.39	- 16.84	11.04	0.96	BCC + B2	
Al <sub>1.25</sub> CoCrFeNi	5.63	7.00	- 13.40	13.34	1.60	BCC	(Ref 56)
Cr <sub>0.25</sub> FeNi <sub>2.75</sub> Al	5.71	8.03	- 13.53	9.31	1.11	FCC + B2	(Ref 57)
Cr <sub>0.5</sub> FeNi <sub>2.5</sub> Al	5.65	7.82	- 13.64	10.12	1.21	FCC + B2	
Cr <sub>0.75</sub> FeNi <sub>2.25</sub> Al	5.59	7.61	- 13.61	10.70	1.29	FCC + B2	
CrFeNi <sub>2</sub> Al	5.53	7.44	- 13.44	11.14	1.37	FCC + BCC + B2	
Cr <sub>1.25</sub> FeNi <sub>1.75</sub> Al	5.46	7.21	- 13.13	11.33	1.45	BCC + B2	
Cr <sub>1.5</sub> FeNi <sub>1.5</sub> Al	5.39	7.03	- 12.68	11.42	1.53	BCC + B2	

In order to study MPEAs in depth and design MPEAs that are better in line with practical production requirements, the researchers summarized the parameters of existing MPEAs and then proposed a phase formation criterion. Zhang (Ref 58) et al. used  $\delta_r$  and  $\Delta H$  to determine whether the solid solution phase (SS), intermetallic compound phase (IM), and amorphous phase appeared in the alloy. Guo (Ref 55) et al. employed the valence electron concentration parameter to forecast the composition of the phase, with  $VEC \geq 8$ , FCC structural solid solution will be developed; when  $VEC \leq 6.87$ , BCC structural solid solution will be formed; if  $6.87 < VEC < 8$ , FCC + BCC structural solid solution will be formed. However, this criterion does not apply to any of the alloys listed in Table 5, including AlCoCrFeNi<sub>3.0</sub> (Ref 39), Al<sub>0.5</sub>CrFeNiTi<sub>0.25</sub> (Ref 54), and Al<sub>1.25</sub>CoCrFeNi (Ref 56). This may be due to its perception of the B2 phase as an ordered BCC phase, but the NiAl phase is an IM. Furthermore, Zhang and Yang (Ref 59) separated the SS and the IM by  $\Omega$  parameters, and only the SS phase appeared in the range of  $\Omega \geq 1.1$  and  $\delta_r < 3.6\%$ , while

there were mixing phases of IM and SS in the range  $1.1 \leq \Omega \leq 10$  and  $3.6\% \leq \delta_r \leq 6.6\%$ . The calculation found that all of the (Ni<sub>x</sub>Al)<sub>65</sub>Cr<sub>10</sub>Mo<sub>5</sub>V<sub>20</sub> alloy systems had  $\delta_r$  greater than 6.6% and  $\Omega$  less than 1.1, but the phase composition was SS + IM, which could be related to considering the B2 phase as an ordered BCC phase (Ref 51), or the criterion needs to be refined further. Simultaneously, data analysis reveals that the majority of the MPEAs with SS + IM structures identified by Zhang et al. contain Cu, and the binary mixing enthalpy of Cu and other constituent elements is relatively high (generally greater than 0). This raises the alloy's overall mixing enthalpy, and  $\Omega$  is likewise affected by the mixing enthalpy. In contrast, the mixing enthalpy and  $\Omega$  values of the constituent elements are modest in this study. By comparing experimental data, Wang (Ref 60) came to the conclusion that  $\Delta H_{mix}$  and  $\delta_r$  are important parameters for a single SS to form in MPEAs. Considering that  $\Omega$  parameters can distinguish between the SS and the IM, and in light of the literature and the work in this paper,  $\Delta H_{mix}$ ,  $\delta_r$ , and  $\Omega$  were used

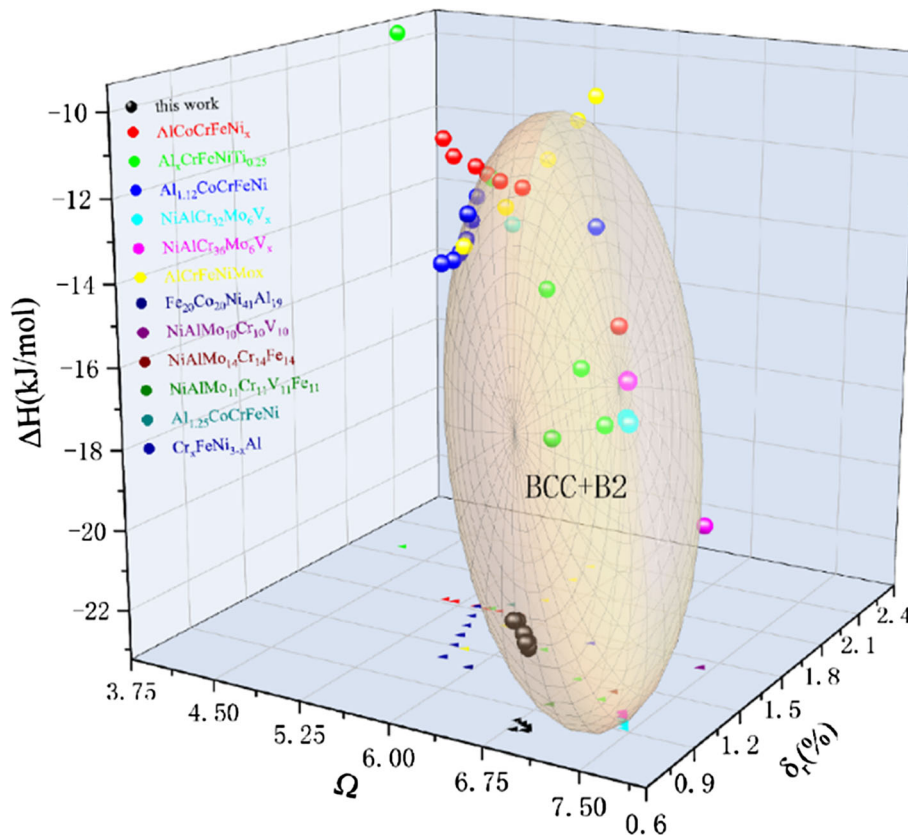


**Fig. 8** Diagram showing the relationship among  $\Delta H_{\text{mix}}$ ,  $\delta_r$  and  $\Omega$

to analyze MPEAs with the BCC + B2 phase concurrently, and the B2 phase was classified as the IM. Figure 8 shows the statistical results of  $\Delta H_{\text{mix}}$ ,  $\delta_r$ , and  $\Omega$  versus alloy phase: when  $\Delta H_{\text{mix}} \leq 12.31(\text{kJ/mol})$ ,  $5.76(\%) \leq \delta_r \leq 7.44(\%)$ , and  $0.75 \leq \Omega \leq 1.53$ , the structure in the MPEA is the BCC + B2 (NiAl) phase. The significance of the criterion is that limiting the atomic size range balances phase separation and solid solution, and negative mixing enthalpy secures the IM phase. Additionally, limiting the  $\Omega$  value allows the system to have a specific mixing entropy, which ensures the formation of solid solutions.

## 4. Conclusions

This study produced MPEAs from  $(\text{Ni}_x\text{Al})_{65}\text{Cr}_{10}\text{Mo}_5\text{V}_{20}$  ( $x = 0.6, 0.8, 1.0, 1.2, 1.4, 1.6$ ). The alloys' solidification microstructures and mechanical properties were examined. The findings are as follows:

- (1) Microstructure of  $(\text{Ni}_x\text{Al})_{65}\text{Cr}_{10}\text{Mo}_5\text{V}_{20}$  MPEAs is both B2 and BCC, which changes from hypereutectic (primary BCC + eutectic,  $x = 0.6, 0.8$ ) to eutectic ( $x = 1.0$ ) and then to hypoeutectic (primary NiAl + eutectic,  $x = 1.2, 1.4, 1.6$ ) as the Ni/Al ratio rises where the BCC phase has more Mo, Cr, and V and the B2 phase has more Ni and Al.
- (2) As the Ni/Al ratio rises, the strength and plasticity of the alloy increase initially and then decrease, owing to precipitation strengthening, fine-grain strengthening, and

B2 phase strengthening. The alloys Ni-1.0, Ni-1.2, Ni-1.4, and Ni-1.6 all exhibit excellent strength and plasticity, with Ni-1.2 having the best overall performance, with fracture strength 3106 MPa, strain at break of 25%, yield strength of 1600 MPa, and hardness of 697 HV. It is a novel structural material with significant potential for application.

- (3) In conjunction with this work and the literature, the following phase prediction criteria of BCC phase + B2(NiAl) phase for the microstructure of multi-principal element alloys are proposed:  $\Delta H_{\text{mix}} \leq 12.31(\text{kJ/mol})$ ,  $5.76(\%) \leq \delta_r \leq 7.44(\%)$ , and  $0.75 \leq \Omega \leq 1.53$ .

## Acknowledgments

The research was financially supported by the Yichang Key Laboratory of Graphite Additive Manufacturing Program (Nos. YKLGAM202001).

## References

1. J.W. Yeh et al., Nanostructured High-Entropy Alloys with Multiple Principal Elements: Novel Alloy Design Concepts and Outcomes, *Adv. Eng. Mater.*, 2004, **6**, p 299–303
2. B. Cantor, I.T.H. Chang, P. Knight and A.J.B. Vincent, Microstructural Development in Equiatomic Multicomponent Alloys, *Mater. Sci. Eng., A*, 2004, **375–377**, p 213–218
3. J. Joseph, N. Stanford, P. Hodgson and D.M. Fabijanic, Understanding the Mechanical Behaviour and the Large Strength/Ductility Differences

- Between FCC and BCC Al<sub>x</sub>CoCrFeNi High Entropy Alloys, *J. Alloy. Compd.*, 2017, **726**, p 885–895
4. F. Otto, A. Dlouhý, C. Somsen, H. Bei, G. Eggeler and E.P. George, The Influences of Temperature and Microstructure on the Tensile Properties of a CoCrFeMnNi High-Entropy Alloy, *Acta Mater.*, 2013, **61**, p 5743–5755
  5. C.-C. Tung, J.-W. Yeh, T.-T. Shun, S.-K. Chen, Y.-S. Huang and H.-C. Chen, On the Elemental Effect of AlCoCrCuFeNi High-Entropy Alloy System, *Mater. Lett.*, 2007, **61**, p 1–5
  6. D.B. Miracle and O.N. Senkov, A Critical Review of High Entropy Alloys and Related Concepts, *Acta Mater.*, 2017, **122**, p 448–511
  7. M.S. Rizi, H. Minouei, B.J. Lee, H. Pouraliakbar, M.R. Toroghinejad and S.I. Hong, Hierarchically Activated Deformation Mechanisms to form Ultra-Fine Grain Microstructure in Carbon Containing FeMn-CoCr Twinning Induced Plasticity High Entropy Alloy, *Mater. Sci. Eng. A*, 2021, **824**, p 141803
  8. M.S. Rizi, H. Minouei, B.J. Lee, M.R. Toroghinejad and S.I. Hong, Effects of Carbon and Molybdenum on the Nanostructural Evolution and Strength/Ductility Trade-off in Fe<sub>40</sub>Mn<sub>40</sub>Co<sub>10</sub>Cr<sub>10</sub> High-Entropy Alloys, *J. Alloy. Compd.*, 2022, **911**, p 165108
  9. H. Pouraliakbar, S.H. Shim, Y.K. Kim, M.S. Rizi, H. Noh and S.I. Hong, Microstructure Evolution and Mechanical Properties of (CoCrNi)<sub>90</sub>(AlTiZr)<sub>5</sub>(CuFeMo)<sub>5</sub> Multicomponent Alloy: A Pathway Through Multicomponent Alloys Toward New Superalloys, *J. Alloy. Compd.*, 2021, **860**, p 158412
  10. S.H. Shim, H. Pouraliakbar, B.J. Lee, Y.K. Kim, M.S. Rizi and S.I. Hong, Strengthening and deformation Behavior of As-cast CoCr-Cu<sub>1.5</sub>MnNi High Entropy Alloy with Micro-/Nanoscale Precipitation, *Mater. Sci. Eng. A*, 2022, **853**, p 143729
  11. Y. Lu et al., Directly Cast Bulk Eutectic and Near-Eutectic High Entropy Alloys with Balanced Strength and Ductility in a Wide Temperature Range, *Acta Mater.*, 2017, **124**, p 143–150
  12. M.A. Hemphill et al., Fatigue Behavior of Al<sub>0.5</sub>CoCrCuFeNi High Entropy Alloys, *Acta Mater.*, 2012, **60**, p 5723–5734
  13. C.-J. Tong et al., Microstructure Characterization of Al<sub>x</sub>CoCrCuFeNi High-Entropy Alloy System with Multiprincipal Elements, *Metall. Mater. Trans. A.*, 2005, **36**, p 881–893
  14. Y. Lu et al., A Promising New Class of High-Temperature Alloys: Eutectic High-Entropy Alloys, *Sci. Rep.*, 2014, **4**, p 6200
  15. Y. Lu, H. Jiang, S. Guo, T. Wang, Z. Cao and T. Li, A New Strategy to Design Eutectic High-Entropy Alloys using Mixing Enthalpy, *Intermetallics*, 2017, **91**, p 124–128
  16. H. Jiang et al., A New Strategy to Design Eutectic High-Entropy Alloys using Simple Mixture Method, *Mater. Des.*, 2018, **142**, p 101–105
  17. Z. Ding, Q. He and Y. Yang, Exploring the Design of Eutectic or Near-Eutectic Multicomponent Alloys: From Binary to High Entropy Alloys, *Sci. China Technol. Sci.*, 2018, **61**, p 159–167
  18. F. He et al., Designing Eutectic High Entropy Alloys of CoCrFeNiNb<sub>x</sub>, *J. Alloy. Compd.*, 2016, **656**, p 284–289
  19. X. Jin, Y. Zhou, L. Zhang, X. Du and B. Li, A New Pseudo Binary Strategy to Design Eutectic High Entropy Alloys using Mixing Enthalpy and Valence Electron Concentration, *Mater. Des.*, 2018, **143**, p 49–55
  20. Z. Tang et al., Aluminum Alloying Effects on Lattice Types, Microstructures, and Mechanical Behavior of High-Entropy Alloys Systems, *Jom*, 2013, **65**, p 1848–1858
  21. J. Zhou and J. Guo, Effect of Ag Alloying on Microstructure, Mechanical and Electrical Properties of NiAl Intermetallic Compound, *Mater. Sci. Eng. A*, 2003, **339**, p 166–174
  22. L. Hu, G. Zhang, W. Hu, G. Gottstein, S. Bogner and A. Bührig-Polaczek, Tensile Creep of Directionally Solidified NiAl-9Mo in situ Composites, *Acta Mater.*, 2013, **61**, p 7155–7165
  23. H. Bei and E. George, Microstructures and Mechanical Properties of a Directionally Solidified NiAl-Mo Eutectic Alloy, *Acta Mater.*, 2005, **53**, p 69–77
  24. D. Johnson, X. Chen, B. Oliver, R.D. Noebe and J. Whittenberger, Processing and Mechanical Properties of in-situ Composites from the NiAlCr and the NiAl (Cr, Mo) Eutectic Systems, *Intermetallics*, 1995, **3**, p 99–113
  25. D. Yu, H. Bei, Y. Chen, E.P. George and K. An, Phase-Specific Deformation Behavior of a Relatively Tough NiAl-Cr (Mo) Lamellar Composite, *Scr. Mater.*, 2014, **84**, p 59–62
  26. L. Sheng, W. Zhang, J. Guo, L. Zhou and H. Ye, Microstructure Evolution and Mechanical Properties' Improvement of NiAl-Cr (Mo)-Hf Eutectic Alloy during Suction Casting and Subsequent HIP Treatment, *Intermetallics*, 2009, **17**, p 1115–1119
  27. S. Milenkovic and R. Caram, Mechanical Properties and Fracture Behavior of Directionally Solidified NiAl-V Eutectic Composites, *Metall. and Mater. Trans. A.*, 2015, **46**, p 557–565
  28. A. Misra and R. Gibala, Room-Temperature Deformation Behavior of Directionally Solidified Multiphase Ni-Fe-Al Alloys, *Metall. and Mater. Trans. A.*, 1997, **28**, p 795–807
  29. X. Ye et al., A New Infinite Solid Solution Strategy to Design Eutectic High Entropy Alloys with B2 and BCC Structure, *Scripta Mater.*, 2021, **199**, p 113886
  30. M. Kellner, J. Hötzer, E. Schoof and B. Nestler, Phase-Field Study of Eutectic Colony Formation in NiAl-34Cr, *Acta Mater.*, 2020, **182**, p 267–277
  31. X. Du, J. Guo and B. Zhou, Superplastic Behavior in Pseudo-Eutectic NiAl-9Mo Alloy, *Mater. Lett.*, 2002, **52**, p 442–447
  32. S. Milenkovic and R. Caram, Growth Morphology of the NiAl-V in situ Composites, *J. Mater. Process. Technol.*, 2003, **143**, p 629–635
  33. H. Okamoto, Supplemental Literature Review of Binary Phase Diagrams: Al-P, B-Ga, B-Nd, Ba-Ga, Bi-Cs, Ca-Ga, Cd-Gd, Cr-Mo, Gd-Ni, Ni-Pb, Ni-Sc, and Sc-Sn, *J. Phase Equilib. Diffus.*, 2015, **36**, p 518–530
  34. H. Okamoto, Supplemental Literature Review of Binary Phase Diagrams: Ag-Li, Ag-Sn, Be-Pu, C-Mn, C-Si, Ca-Li, Cd-Pu, Cr-Ti, Cr-V, Cu-Li, La-Sc, and Li-Sc, *J. Phase Equilib. Diffus.*, 2017, **38**, p 70–81
  35. J. Westbeek, Temperature Dependence of Hardness of the Equi-Atomic Iron Group Aluminides, *J. Electrochem. Soc.*, 1956, **103**, p 54
  36. K. Hahn and K. Vedula, Room Temperature Tensile Ductility in Polycrystalline B2 NiAl, *Scr. Metall.* 23 (1989)
  37. Y. Qi, J. Guo, G. Li, Effect of Stoichiometry on Microstructure and Mechanical Properties of NiAl-Mo(Nb)Intermetallic(in Chinese). (2003)
  38. X. Jin et al., A New CrFeNi<sub>2</sub>Al Eutectic High Entropy Alloy System with Excellent Mechanical Properties, *J. Alloy. Compd.*, 2019, **770**, p 655–661
  39. L. Cao et al., Microstructural Evolution, Phase Formation and Mechanical Properties of Multi-Component AlCoCrFeNi<sub>x</sub> Alloys, *Appl. Phys. A*, 2019, **125**, p 1–11
  40. M. Wang et al., A Novel High-Entropy Alloy Composite Coating with Core-Shell Structures Prepared by Plasma Cladding, *Vacuum*, 2021, **184**, p 109905
  41. S. Wang et al., Nano-Phase Formation Accompanying Phase Separation in Undercooled CoCrCuFeNi-3 at.% Sn High Entropy Alloy, *Mater. Charact.*, 2018, **144**, p 516–521
  42. Z. Shang et al., Effects of V Addition on the Solidification Microstructures and Room Temperature Compression Properties of NiAl-Cr (Mo) Hypereutectic Alloy, *Vacuum*, 2020, **179**, p 109507
  43. Y. Dong, Y. Lu, J. Kong, J. Zhang and T. Li, Microstructure and Mechanical Properties of Multi-component AlCrFeNiMo<sub>x</sub> High-Entropy Alloys, *J. Alloy. Compd.*, 2013, **573**, p 96–101
  44. M. Alger, *Polymer Science Dictionary*, Springer, Berlin, 1996
  45. J. He et al., A Precipitation-Hardened High-Entropy Alloy with Outstanding Tensile Properties, *Acta Mater.*, 2016, **102**, p 187–196
  46. J. He et al., Effects of Al Addition on Structural Evolution and Tensile Properties of the FeCoNiCrMn High-Entropy alloy System, *Acta Mater.*, 2014, **62**, p 105–113
  47. C. Lee et al., Lattice Distortion in a Strong and Ductile Refractory High-Entropy Alloy, *Acta Mater.*, 2018, **160**, p 158–172
  48. E. Hall, The Deformation and Ageing of Mild Steel: III Discussion of Results, *Proc. Phys. Soc. London Sect. B*, 1951, **64**, p 747
  49. L. Yu et al., Precise Design Strategy of FeNiCrMo Eutectic High-Entropy Alloys, *J. Market. Res.*, 2022, **21**, p 3207–3219
  50. D. Wu, J. Zhang, J. Huang, H. Bei and T.-G. Nieh, Grain-Boundary Strengthening in Nanocrystalline Chromium and the Hall-Petch Coefficient of Body-Centered Cubic Metals, *Scripta Mater.*, 2013, **68**, p 118–121
  51. Y. Dong, S. Chen, J. Wang and K. Jin, Research Progress in Multi-Principal Element Alloys Containing Coherent BCC/B2 Structure(in Chinese), *J. Mater. Eng.*, 2021, **49**, p 1–9

52. L. Wang et al., Microstructure and Mechanical Property of Novel NiAl-based Hypoeutectic/Eutectic/Hypereutectic High-Entropy Alloy, *Intermetallics*, 2022, **143**, p 107476
53. J. Guo, C. Cui, Y. Chen, D. Li and H. Ye, Microstructure, Interface and Mechanical Property of the DS NiAl/Cr (Mo, Hf) Composite, *Intermetallics*, 2001, **9**, p 287–297
54. S. Liu, M. Gao, P. Liaw and Y. Zhang, Microstructures and mechanical properties of  $\text{Al}_x\text{CrFeNiTi}_{0.25}$  alloys, *J. Alloys Compd.*, 2015, **619**, p 610–615
55. S. Guo, C. Ng, J. Lu and C. Liu, Effect of Valence Electron Concentration on Stability of FCC or BCC Phase in High Entropy Alloys, *J. Appl. Phys.*, 2011, **109**, p 103505
56. M. Izadi, M. Soltanieh, S. Alamolhoda, S. Aghamiri and M. Mehdizade, Microstructural Characterization and Corrosion Behavior of  $\text{Al}_x\text{CoCrFeNi}$  High Entropy Alloys, *Mater. Chem. Phys.*, 2021, **273**, p 124937
57. W. Zhang, X. Ye, D. Xu, C. Liu, D. Fang and B. Li, Microstructures and Properties of  $\text{Cr}_x\text{FeNi}_{(3-x)}\text{Al}$  High-Entropy Alloys, *Appl. Phys. A*, 2022, **128**, p 1–9
58. Y. Zhang, Y.J. Zhou, J.P. Lin, G.L. Chen and P.K. Liaw, Solid-Solution Phase Formation Rules for Multi-Component Alloys, *Adv. Eng. Mater.*, 2008, **10**, p 534–538
59. X. Yang and Y. Zhang, Prediction of High-Entropy Stabilized Solid-Solution in Multi-Component Alloys, *Mater. Chem. Phys.*, 2012, **132**, p 233–238
60. Z. Wang, S. Guo and C.T. Liu, Phase Selection in High-Entropy Alloys: From Nonequilibrium to Equilibrium, *Jom*, 2014, **66**, p 1966–1972

**Publisher's Note** Springer Nature remains neutral with regard to jurisdictional claims in published maps and institutional affiliations.

Springer Nature or its licensor (e.g. a society or other partner) holds exclusive rights to this article under a publishing agreement with the author(s) or other rightsholder(s); author self-archiving of the accepted manuscript version of this article is solely governed by the terms of such publishing agreement and applicable law.